ADVANCED MATERIALS
www.advmat.de

A Mechanically Robust and Versatile Liquid-Free Ionic Conductive Elastomer

Burebi Yiming, Ying Han, Zilong Han, Xinning Zhang, Yang Li, Weizhen Lian, Mingqi Zhang, Jun Yin, Taolin Sun,* Ziliang Wu, Tiefeng Li, Jianzhong Fu, Zheng Jia,* and Shaoxing Qu*

Soft ionic conductors, such as hydrogels and ionogels, have enabled stretchable and transparent ionotronics, but they suffer from key limitations inherent to the liquid components, which may leak and evaporate. Here, novel liquid-free ionic conductive elastomers (ICE) that are copolymer networks hosting lithium cations and associated anions via lithium bonds and hydrogen bonds are demonstrated, such that they are intrinsically immune from leakage and evaporation. The ICEs show extraordinary mechanical versatility including excellent stretchability, high strength and toughness, self-healing, quick self-recovery, and 3D-printability. More intriguingly, the ICEs can defeat the conflict of strength versus toughness—a compromise well recognized in mechanics and material science—and simultaneously overcome the conflict between ionic conductivity and mechanical properties, which is common for ionogels. Several liquid-free ionotronics based on the ICE are further developed, including resistive force sensors, multifunctional ionic skins, and triboelectric nanogenerators (TENGs), which are not subject to limitations of previous gel-based devices, such as leakage, evaporation, and weak hydrogel–elastomer interfaces. Also, the 3D printability of the ICEs is demonstrated by printing a series of structures with fine features. The findings offer promise for a variety of ionotronics requiring environmental stability and durability.

Soft machines have made the transition from conventional electronics to ionotronics, exemplified by the emergence of a variety of ionotronic devices, such as stretchable touchpads,[1] skin-like sensors,[2–4] ionic cables,[5,6] nanogenerators,[7] soft diodes,[8] and flexible displays.[9] Unlike electronic-based devices, which rely mostly on electrons to conduct electricity, ionotronic devices function predominantly by the motion of ions, just as what living organisms do.[10] With the advent of soft ionotronic devices, there is an urgent need for the development of novel ionic conductors. To meet the stringent requirements of flexible electronics and soft machines, ionic conductors are naturally desired to possess excellent mechanical properties—including ruggedness and self-healing capability—and attributes such as optical transparency and high conductivity. Hydrogels containing mobile ions, which are stretchable, transparent, and conductive, are considered as promising candidates for ionic conductors, and have enabled many

B. R. B. Yiming, Z. L. Han, M. Q. Zhang, Prof. T. F. Li, Prof. Z. Jia, Prof. S. X. Qu
Key Laboratory of Soft Machines and Smart Devices of Zhejiang Province
Center for X-Mechanics
Department of Engineering Mechanics
Zhejiang University
Hangzhou 310027, China
E-mail: zheng.jia@zju.edu.cn

Y. Han, Y. Li, Prof. J. Yin, Prof. J. Z. Fu
The State Key Laboratory of Fluid Power and Mechatronic Systems
Key Laboratory of 3D Printing Process and Equipment of Zhejiang Province
School of Mechanical Engineering
Zhejiang University
Hangzhou 310027, China
E-mail: junyin@zju.edu.cn

The ORCID identification number(s) for the author(s) of this article can be found under https://doi.org/10.1002/adma.202006111.

X. N. Zhang, Prof. Z. L. Wu
Ministry of Education Key Laboratory of Macromolecular Synthesis and Functionalization Department of Polymer Science and Engineering
Zhejiang University
Hangzhou 310027, China

W. Z. Lian, Prof. T. L. Sun
South China Advanced Institute for Soft Matter Science and Technology
South China University of Technology
Guangzhou 510640, China
E-mail: suntl@scut.edu.cn

DOI: 10.1002/adma.202006111

 © 2021 Wiley-VCH GmbH

hydrogel-based applications such as ionic skins,[11–13] soft actuators,[14] and energy harvesting devices.[15,16] These devices, however, often suffer from limitations inherent to hydrogels, which are unstable due to rapid evaporation of water in ambient conditions and do not adhere well to other materials.[10] Introducing chemicals or salts in hydrogels can only retard but not prevent the dehydration of hydrogels.[17,18] Sealing and coating hydrogel devices with hydrophobic materials like elastomers are more effective at retaining water but usually require complicated procedures to enable strong hydrogel/elastomer adhesion.[11,19,20] In recent years, ionic conductors based on ionic liquids (ILs), aka ionogels, have garnered great attention, owing to their non-volatile nature, excellent thermal stability and ionic conductivity.[3,21–24] The common problem faced in this system is the leakage of IL when subjected to mechanical forces (e.g., squeezing).[25] Strategies such as fabricating conductive nanochannels and employing ILs that can form hydrogen bonds with polymer chains have been proposed to prevent the loss of ILs.[25,26] Meanwhile, the tradeoff between ionic conductivity and mechanical robustness should be addressed as well—in general, using a large amount of ILs can enhance the conductivity of gels but cause degradation of mechanical properties (e.g., strength and modulus).[3,22,25] More recently, ionotronic diodes and transistors have been demonstrated with the use of ionic conductive elastomers that are comprised entirely of polymer networks and mobile ions and contain no liquid components, such that these devices are non-volatile without the hassles of leaking liquid materials.[27] Thus far, the report of mechanically robust ionic conductive elastomers is still rare:[28] demonstrated liquid-free ionic conductive elastomers exhibit limited stretchability and self-healing capability,[27,29] incompatible with the stringent requirements of durability for soft machines and wearable electronics.

In the present study, inspired by polymer electrolytes for solid-state lithium-ion batteries,[30] we synthesize a novel liquid-free ionic conductive elastomer (ICE)—an elastomer hosting lithium (Li) cations and associated anions via lithium bonds and hydrogen bonds, respectively. The material is highly stretchable, up to a uniaxial strain of ≈1744%, rendering it one of the most stretchable liquid-free ICEs reported so far. This material also features high strength and toughness (resistance to crack propagation), self-healing behavior, quick self-recovery, 3D-printability, as well as thermal stability and optical transparency. In sharp contrast to IL-based ionic conductors, mechanical properties and ionic conductivity of the liquid-free ICE increase simultaneously with the concentration of lithium ions, in virtue of hydrogen bonds and lithium bonds between the lithium salts and polymer chains. In particular, we can attain both improved strength and toughness, two mechanical properties that are often mutually exclusive in material design (i.e., the increase of strength usually comes at a price of sacrificing toughness),[31,32] defeating the well-recognized conflict of strength versus toughness.[32] To demonstrate the applications of the liquid-free ICE to ionotronics, we construct a stretchable resistive-type sensor, a capacitive-type ionic skin, and a triboelectric nanogenerator (TENG), which can convert multiple mechanical and environmental stimuli—including stretch, touch, and temperature change—into electrical signals. These solvent-free devices consist entirely of ICEs (electrodes) and ion-free elastomers (dielectrics), such that they possess much better environmental stability and stronger electrode/dielectric interfaces than their gel-based counterparts. Another advantage of the material is 3D-printability. For the first time, we demonstrate the capability of printing liquid-free ICEs into various complicated shapes, showing the outstanding processability of the ICE. These desirable traits make the material a suitable candidate for ionotronic-based devices and machines.

To make the ICE, lithium bis(trifluoromethane)sulfonimide (LiTFSI), a lithium salt widely used in polymer electrolytes for lithium-ion batteries, is dissolved in liquid binary mixtures of ethylene glycol methyl ether acrylate (MEA) and isobornyl acrylate (IBA). The molar concentration C of LiTFSI is taken to be 0.5 M in this work unless otherwise noted. Using 0.0052 M benzophenone, a photoinitiator that is soluble in the liquid monomers, the ICE is then formed by the free-radical copolymerization of the mixtures of acrylate monomers without using any organic solvents. Thus, the ICE consists entirely of a crosslinked copolymer network, that is, P(MEA-*co*-IBA),[33] as well as mobile lithium ions and associated anions (**Figure 1**a and Figure S1, Supporting Information), and is liquid-free. We choose P(MEA-*co*-IBA) with $F = 0.2$—F denotes the molar fraction of IBA monomer in the copolymer backbone—as the copolymer network since it is highly stretchable (Figure S2, Supporting Information) and can endow the ICE with extraordinary mechanical properties. In the ICE, lithium ions are located at suitable coordinate sites (e.g., oxygen atoms in the ester groups) along the polymer chains and can migrate from one site to another under applied electric fields, thereby imparting ionic conductivity to the ICE.

Small-angle X-ray scattering (SAXS) and wide-angle X-ray scattering (WAXS) are performed to investigate the microstructure of the ICE. The ICE has an amorphous structure and hence no phase separation is observed, indicating that LiTFSI is homogeneously dispersed in the ICE, and MEA and IBA are randomly arranged along the copolymer chains (Figure 1b and Figure S3, Supporting Information). Owing to the amorphous nature, the liquid-free ICE is optically transparent (Inset of Figure 1b and Figure S4a, Supporting Information), such that a QR code covered by an ICE film about 0.5 mm thick can be readily scanned and recognized by a QR reader (Video S1, Supporting Information). The average transmittance of the 0.5 mm thick ICE film is about 90% (Figure S4b, Supporting Information). The ICE possesses a considerable fracture strain of ≈1640% (Figure 1c), higher than the ≈1400% value of the pure copolymer P(MEA-*co*-IBA) of $F = 0.2$ that contains no LiTFSI (Figure S2, Supporting Information). It is worth noting that this is one of the most stretchable liquid-free ICEs reported. The liquid-free ICE also exhibits high thermal stability, as confirmed by the thermogravimetric analysis (TGA) (Figure 1d and Figure S5a, Supporting Information). As evident in Figure 1d, the TGA measurements of ICE of $C = 0.5$ M show a negligible weight loss (less than 3%) before the temperature reaches 150 °C (Inset of Figure 1d), demonstrating a stable working temperature which is much higher than that of hydrogel-based ionic conductors (Figure S5a, Supporting Information). Moreover, the ICE has a glass transition temperature (T_g) of −14.4 °C (Figure 1e), above which the ICE is stretchable and conductive, as measured by the differential scanning calorimetry (DSC). We found that T_g of the ICE is mainly determined by

© 2021 Wiley-VCH GmbH

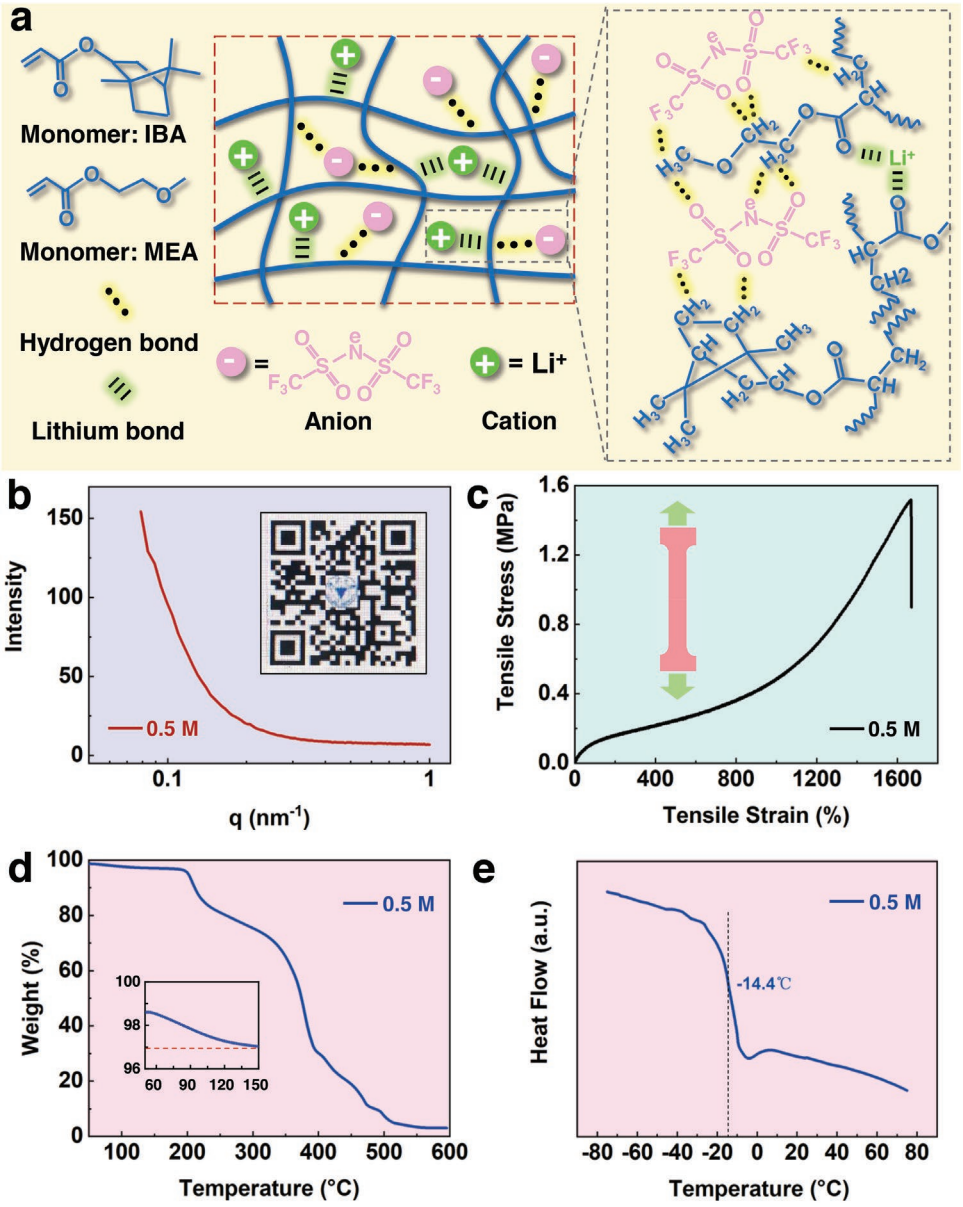

Figure 1. Schematics and physical properties of the liquid-free ionic conductive elastomer (ICE). a) Schematic illustration of the molecular design of the liquid-free ICE, which consists entirely of a crosslinked copolymer network of P(MEA-*co*-IBA), mobile lithium ions, and associated anions. b) The SAXS profile of the ICE. No phase separation is observed. Inset: a QR code covered by an ICE film, showing the optical transparency of the material. c) The stress–strain curve of the ICE until failure. The fracture strain is ≈1640%. d) The TGA results of the ICE, showing high thermal stability with decomposition temperature close to 200 °C. Inset: TGA results before the temperature reaches 150 °C. e) The DSC curve. The glass transition temperature is about −14.4 °C. In all the experiments, $F = 0.2$ and $C = 0.5$ M.

that of the copolymer backbone P(MEA-*co*-IBA), while also affected by the molar concentration of LiTFSI—the higher the content of LiTFSI, the lower the T_g (Figure S5b, Supporting Information). Based on the results of TGA and DSC, it can be concluded that the liquid-free ICE exhibits a wide operating temperature window (e.g., from −14.4 to 200 °C for $C = 0.5$ M) superior to most polyelectrolyte hydrogels. The ICEs also have good humidity stability, since the polymer matrix is hydrophobic (Figure S6, Supporting Information), and the incorporation of lithium salts only induces little water absorption (Figure S7, Supporting Information).

By tuning the molar concentration of LiTFSI, a series of liquid-free ICEs with distinct mechanical properties are synthesized. Mechanical properties including stretchability, fracture toughness, strength, and Young's modulus of the samples are extracted from mechanical tests (Figure S8, Supporting Information) and shown in **Figure 2**a–d, respectively. All the prepared ICEs, of molar concentration C ranging from 0 M (i.e., the pure copolymer) to 2.0 M, possess superb stretchability, with their uniaxial fracture strains higher than 1400% (Figure 2a). Among all the samples, the ICE of $C = 1.0$ M exhibits the highest stretch capability with the strain at break

© 2021 Wiley-VCH GmbH

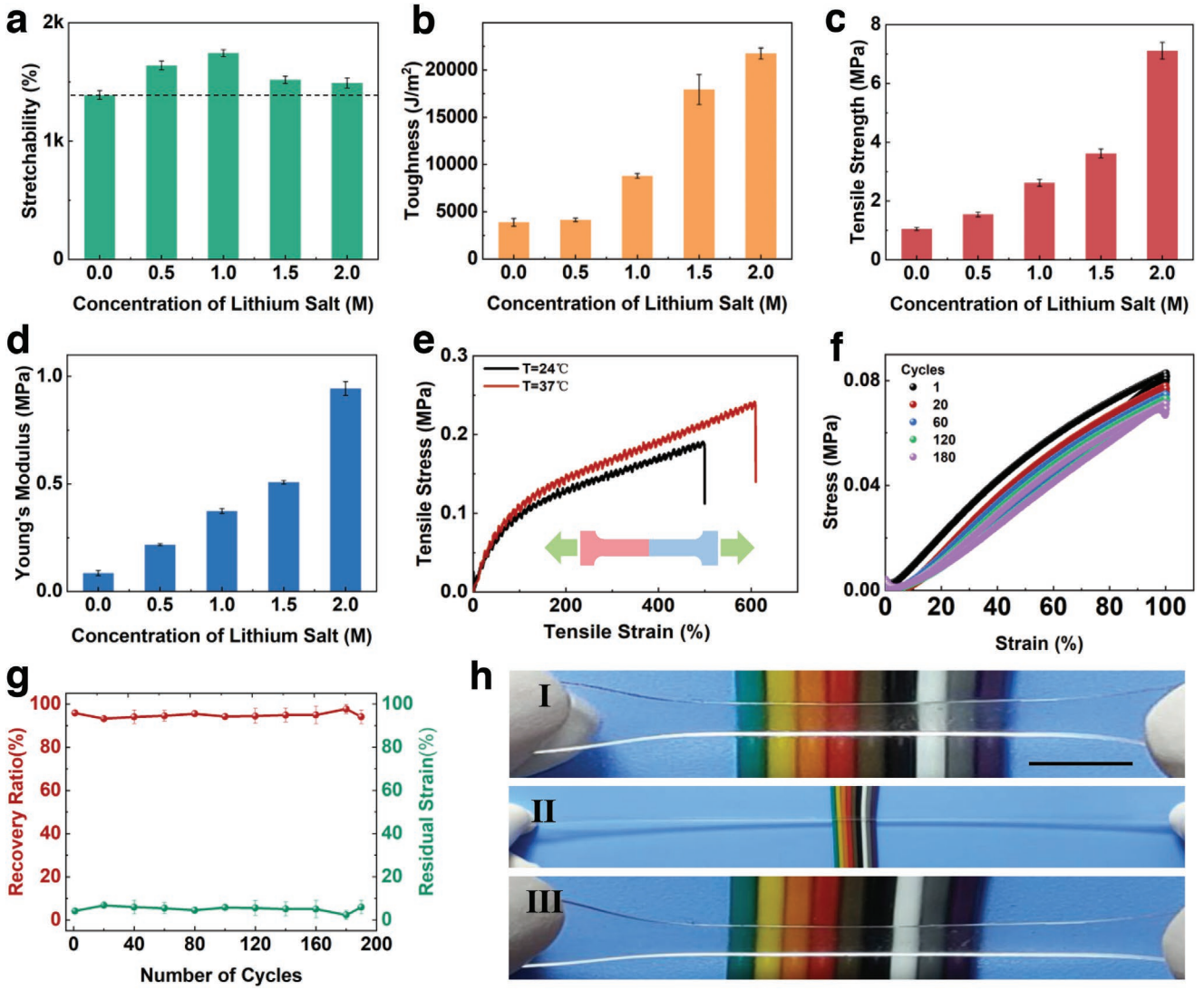

Figure 2. Mechanical properties of the liquid-free ICE. a) Stretchability, b) fracture toughness, c) fracture strength, and d) Young's modulus of ICEs with various LiTFSI concentration values—from $C = 0$ to 2.0 M. It is noteworthy that the liquid-free ICEs defeat the conflict between strength and toughness, which has been well recognized in material science, as well as the conflict of conductivity versus mechanical properties (e.g., strength and modulus) for ionogels. e) Stress–strain curves of self-healed samples after 24 h healing at 24 °C and 37 °C. f) Stress–strain curves of the ICE subject to cyclic loadings. g) Residual strain and recovery ratio plotted versus the loading/unloading cycles. h) Photographs of an ICE before (I), during (II), and after (III) stretching. After being stretched to ten times its original length, the ICE recovers nearly its original length immediately, demonstrating a fast self-recovery behavior (scale bar: 5 mm). The molar concentration of LiTFSI is fixed to be $C = 0.5$ M in all above tests unless otherwise noted.

being 1744%. It is noteworthy that all the ICEs in this work (with different content of LiTFSI) demonstrate higher stretchability than most liquid-free ICEs reported so far,[27–29] owing to the long-chain network. The quest for materials of both high strength and fracture toughness is perpetual. Nevertheless, simultaneously enhancing strength and toughness in advanced materials design remains challenging as these two mechanical properties usually contradict each other: stronger materials tend to be more brittle (less tough),[34] whereas lower-strength materials can deform more readily and tend to be more tough.[35] For a given material, increasing one of the two properties often comes at a price of sacrificing the other one.[36,37] This tradeoff between strength and toughness has been well recognized in mechanics and material science.[32] In this work, as the molar concentration of LiTFSI changes from 0 to 2.0 M, the strength of the ICE increases monotonically from 1.05 to 7.12 MPa (Figure 2b); the fracture toughness increases from 3897 to 21 752 J m^{-2} (Figure 2c). That is, surprisingly, both the strength and toughness of the ICE increase simultaneously (roughly 6.8 and 5.6 times, respectively) as the content of the lithium salt increases (from $C = 0$ to 2.0 M), breaking the inverse relation between strength and toughness. To this end, it can be concluded that, for the liquid-free ICE in this work, there is no conflict between strength and toughness, a highly desirable feature in advanced material design. Further measurements of the work of fracture reveal the similar trend: the work of fracture increases about six times from 5.87 to 35 MJ m^{-3} (Figure S9, Supporting Information), the latter represents an

© 2021 Wiley-VCH GmbH

unprecedented value for ICEs.[36] The fractocohesive length of the ICEs, defined as the ratio of toughness over work of fracture,[38] ranges from 0.46 to 0.99 mm (Table S1, Supporting Information), comparable to values typical of elastomers such as VHB.[39] That is, strength and work of fracture of the ICEs are insensitive to any flaw of the size smaller than these values. In addition to excellent stretchability, toughness, and strength, the ICEs exhibit tunable Young's modulus ranging from 86 to 944 kPa (Figure 2d), comparable to that of biological tissues, such as skins and cartilages. Notably, IL-based ionic conductors generally face a tradeoff between conductivity and mechanical properties (strength and Young's modulus)—attaining a higher conductivity requires the addition of more ionic liquids, which inevitably causes degradation in mechanical strength and Young's modulus.[3,22,24,25] In stark contrast, with increasing content of lithium salts, the liquid-free ICEs in this work exhibit both higher Young's modulus and enhanced mechanical strength (Figure 2c,d), overcoming the conflict between conductivity and mechanical robustness, which is typical of IL-based gels.

Given that the liquid-free ICEs consist of densely packed polymer chains (compared with sparsely dispersed chains in ionogels and hydrogels) with ions distributed among them (Figure 1a), the corresponding toughening, strengthening and stiffening mechanisms of the liquid-free ICEs can be understood as follows. At the molecular scale, dense arrays of hydrogen bonds form between the anions and copolymer network, with the hydrogen atoms in the P(MEA-*co*-IBA) chains acting as hydrogen bond donors and the electronegative atoms (such as F and N) in the TFSI anions serving as the acceptors.[26] In addition, a large number of lithium bonds formed between lithium cations and carbonyl oxygens on polymer chains are confimed by attenuated total reflectance Fourier transform infrared spectroscopy (Figure S10, Supporting Information). Lithium bonds are much stronger than hydrogen bonds.[40] Stretching the ICEs causes relative sliding among polymer chains, which involves a cascade of repeated hydrogen bond and lithium bond breaking/reforming events and dissipates a significant amount of energy, thus producing a much higher toughness than that of pure P(MEA-*co*-IBA) copolymer. Consequently, the fracture toughness of the ICE increases with the molar concentration of LiTFSI, as the number of hydrogen bonds and lithium bonds is proportional to the content of lithium salts. This molecular-level toughening mechanism is evidenced by the tensile testing of ICEs: With a higher concentration of LiTFSI, the ICEs exhibit larger hysteresis during loading–unloading cycles (Figure S11, Supporting Information), indicating enhanced energy dissipation due to increasing number of hydrogen bonds and lithium bonds. Moreover, via forming physical bonds with neighboring chains, Li cations and TFSI anions act like physical links among copolymer chains. The enormous number of Li cations and TFSI anions, and associated physical bonds, can effectively increase the material's strength and stiffness—in a fashion similar to that increasing number of crosslinks stiffen and strengthen a polymer network. In other words, the higher the concentration of LiTFSI, the more hydrogen bonds and lithium bonds, the stronger and stiffer the ICEs.

Flexible and wearable ionotronic devices are often subject to large and repeated external forces that may cause mechanical damage (e.g., scratch, cut, etc.) to the materials, therefore, developing ICEs with self-healing capability is necessary to enhance the lifetime of ionotronic devices. Thus far, liquid-free ICEs reported are often not self-healable, however.[36] In contrast, our highly-stretchable ICEs show good self-healing abilities (Figure 2e), owing to the high mobility of the copolymer chains. After cutting the sample into two separate pieces and bringing them back into contact gently, polymer chains can diffuse across the interface over time and form topological entanglements with the network on the other side, thereby mechanically healing the cut sample in ambient conditions. The tensile stress–strain curves of samples ($C = 0.5$ M) after 24 h healing at 24 and 37 °C are presented in Figure 2e. The corresponding stretchability values of the healed samples are ≈500% and ≈610%, respectively, demonstrating a self-healing efficiency between 30–40%. The healing efficiency is lower than some gel-based self-healable systems since ICEs are much stiffer than gels and heal themselves by forming physical entanglements between chains, rather than via the reformation of reversible crosslinks or bonds which occurs in many highly healable gels. Furthermore, the cycling stability and reversibility of the materials also strongly affect the durability of ionotronic devices. We perform cyclic tensile tests with the uniaxial strain cycling between 0% and 100%, which shows similar stress–strain curves up to 190 consecutive cycles (Figure 2f), indicating good cyclic stability. The excellent mechanical reversibility of the ICE is quantitatively characterized by the low residual strain and high recovery ratio: A low residual strain level (≈5%)—the corresponding recovery ratio is ≈95%—is observed during the 190 successive cycles (Figure 2g). Figure 2h shows that a sample of liquid-free ICE is stretched to roughly ten times its original length. After the applied stretch is released, the sample immediately returns to nearly its initial state, demonstrating fast self-recovery behavior. These results suggest that the stretchable liquid-free ICEs possess superb durability (e.g., self-healing capability, cyclic stability, and fast self-recovery).

Apart from the excellent mechanical properties, the liquid-free ICEs also have good ionic conductivity. Herein, the conductivity is measured in ambient conditions and determined by $\sigma = L/(AR)$, with L being the sample length, A the cross-sectional area of the sample, and R the bulk resistance. The conductivity of the ICEs increases from 4.20×10^{-4} to 5.28×10^{-3} Sm^{-1} as the salt concentration increases from $C = 0.5$ to 2.0 M (**Figure 3**a and Table S2, Supporting Information), since the ionic conductivity is typically proportional to the effective number of mobile ions. Additionally, the liquid-free ICEs show higher conductivity as the temperature increases (Figure 3b and Table S3, Supporting Information). For example, the ICE with salt concentration of $C = 0.5$ M has a conductivity of 1.59×10^{-4} Sm^{-1} at 20 °C and 1.65×10^{-3} Sm^{-1} at 80 °C. The temperature-sensitive conductivity can be understood as follows: elevated temperature leads to greater segmental motion of polymer chains and facilitates the ion transport, thereby producing a higher conductivity. The ICEs also demonstrate stable conductivity in ambient conditions. Figure 3c displays the ionic conductivity of the ICEs over 1 week (Table S4, Supporting Information). Samples with LiTFSI concentration of 0.5 and 1.0 M demonstrate desirable conductivity during the period of testing. In contrast, it has been reported that hydrogels (e.g., polyacrylamide/NaCl

© 2021 Wiley-VCH GmbH

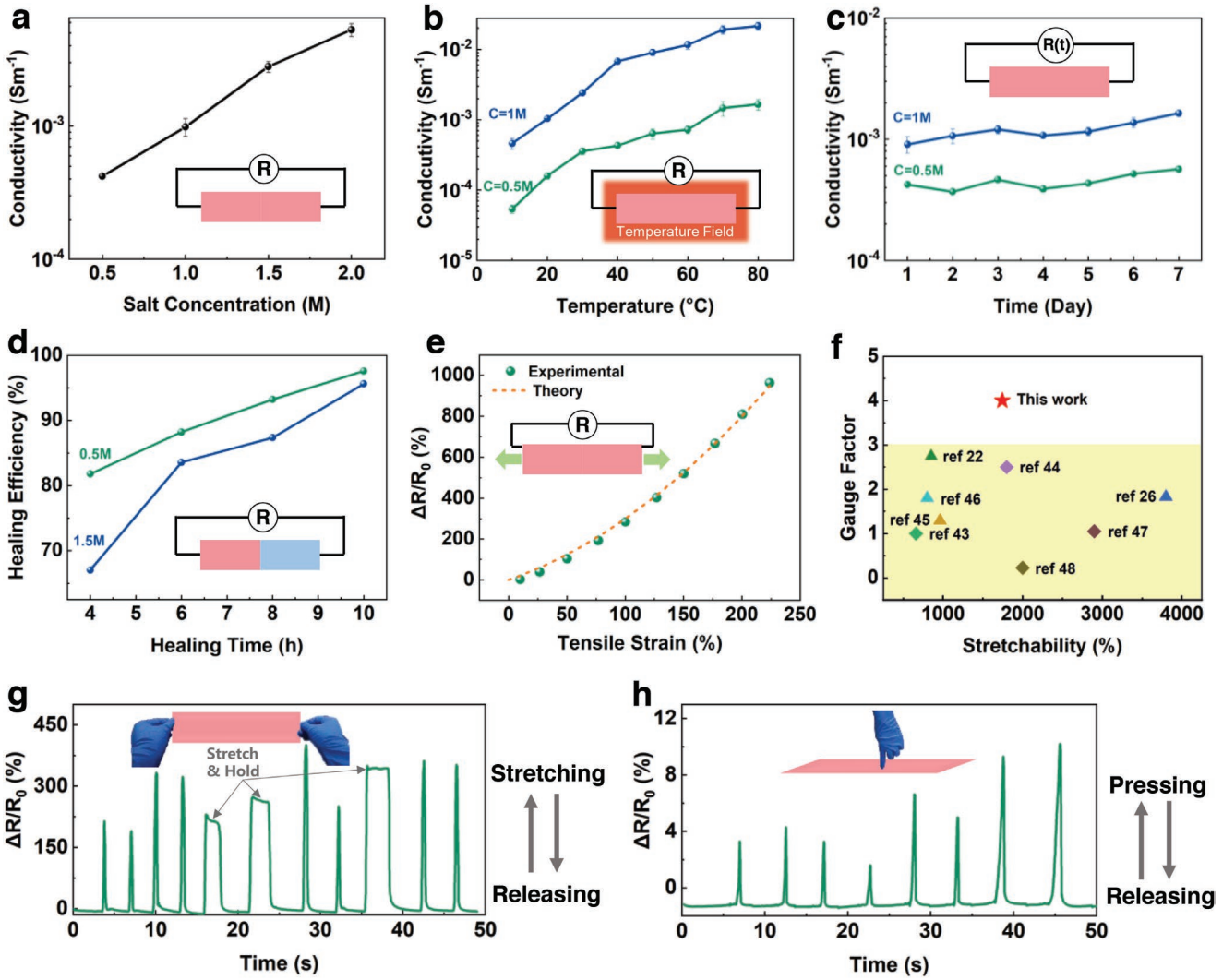

Figure 3. The electrochemical performances of the liquid-free ICE. a) Ionic conductivity of the ICEs with different lithium salt concentrations. b) Temperature-dependent ionic conductivity of samples containing different salt contents. c) The conductivity of ICEs at room temperature for 7 days. d) Capacity of restoring ionic conductivity after cut. The healing efficiency in conductivity is plotted as a function of the healing time, demonstrating 97% of conductivity recovery in 10 h. e) Relative change in resistance versus tensile strain. The green dots denote the experimental data, in good agreement with the theoretical prediction represented by the dashed line. f) Comparison of the liquid-free ICE in this work with previously reported ionic strain sensors in terms of gauge factor and stretchability. Squares and triangles correspond to hydrogel-based and ionogel-based systems, respectively. g,h) Resistance change of the ICE-based strain sensor versus time in response to intermittent stretching (g) and pressure (h) stimuli, demonstrating the versatility of the sensor. The molar concentration of LiTFSI is fixed to be $C = 0.5$ M in the tests unless otherwise noted.

hydrogels) lose 99% of its conductivity after 24 h in air, owing to fast dehydration; the conductivity of PAA/IL ionogels also shows a decrease of 34% in 24 h in ambient conditions, because of the leakage of ionic liquid.[25] The ICEs also demonstrate good conductivity in dry conditions (Table S5, Supporting Information). Mechanical and electrical self-healing properties are critical to the durability of both electronic and ionic conductors.[41,42] The liquid-free ICEs in this work are capable of restoring not only the mechanical properties but ionic conductivity as well. The ICE is cut into half and then placed together gently. Figure 3d shows the conductivity of the cut sample during the self-healing process. Right after cutting, the conductivity of the cut sample is much lower than that of the pristine ICE, despite that the two halves are in physical contact. The conductivity returns to 97% of the initial value in 10 h, showing autonomic electrical self-healing capability after damage (Figure 3d).

Existing ionotronic devices, such as stretchable sensors, artificial skins, and soft actuators, are predominantly based on hydrogels and ionogels, which contain a large quantity of liquid components. By exploiting the non-volatile nature of the ICE, coupled with its mechanical durability and ionic conductivity, we demonstrate liquid-free resistive sensors, which are inherently not subject to leakage and evaporation. To illustrate the working principle of the sensor, we first derive the relation between resistance change of the ICE and deformation. The ideal elastomer model assuming constant volume and resistivity is adopted.[11] When an ICE sheet (i.e., the resistive sensor) is stretched by a factor of λ, the cross-sectional area scales

© 2021 Wiley-VCH GmbH

by factor $1/\lambda$, and hence the resistance R of the ICE scales as $R = R_0 \lambda^2$ (More details are given in Supporting Information), where R_0 denotes the initial resistance before stretching. One notes that the stretch ratio λ is related to the tensile strain by $1 + \varepsilon$, such that the relative change in resistance is $\Delta R/R_0 = (1 + \varepsilon)^2 - 1$. Figure 3e shows the relative change in resistance, $\Delta R/R_0$, as a function of the applied tensile strain ε up to ≈220%. As the ICE sheet is stretched, the experimentally measured resistance increases in a quadratic manner as the applied strain increases, and matches very well with the theoretical prediction above (Figure 3e). The drastic change of bulk resistance in response to stretch indicates the feasibility of the material as a resistive strain sensor. The gauge factor (GF, defined as $GF = d(\Delta R/R_0)/d\varepsilon$) of the sensor increases with the applied strain: The GF is 2.02 at 1% strain, and increases to 4 and 6 at 100% and 200% strains, respectively. In Figure 3f, we compare the ICE-based resistive sensor in this work to those previously reported—They are based on hydrogels and ionogels. The GF values of all sensors are evaluated at ≈100% strain to achieve a fair comparison. In terms of gauge factor and stretchability, the two key metrics for stretchable sensors, the liquid-free resistive sensor in this work outperforms most ionotronic resistive sensors.[22,26,43–48] Figure 3g and Video S2, Supporting Information, show the resistance variation of the sensor under a series of stretch stimuli. The performance of the stretch resistive sensor is stable and reversible over many cycles (Figure S12, Supporting Information). The ICE-based resistive sensor is further applied to monitor pressure produced by touch motions. A series of strong resistance peaks are observed when touch pressure is exerted on the surface of the resistive sensor (Figure 3h and Video S3, Supporting Information), revealing the strong stress-sensitive behavior of the ICE-based resistive sensors (Figure S13, Supporting Information).

Another representative ionotronic device is the ionic skin, a capacitive sensor consisting of a dielectric elastomer—for example, acrylic elastomer VHB or poly(dimethylsiloxane) (PDMS)—sandwiched between two ionic conductors (i.e., electrodes). The two electrodes are connected to a capacitive meter through two metal wires. When external forces (i.e., stretch or pressure) deform the skin, the capacitance measured by the capacitive meter increases, enabling the ionic skin to sense the deformation. Based on this concept, a variety of ionic skins have been reported,[11,12] mostly employing polyelectrolyte hydrogels and ionogels as the ionic conductors. In this work, we use the ICE as the ionic electrodes, making a liquid-free non-volatile ionic skin, which comprises a dielectric elastomer (i.e., pure P(MEA-*co*-IBA) copolymer) sandwiched between two ICEs (i.e., P(MEA-*co*-IBA) copolymer containing LiTFSI of 1.5 M) (**Figure 4**a). The novel ionic skin is intrinsically not subject to leakage and, more importantly, possesses strong elastomer-ICE adhesion, in sharp contrast to the poor elastomer-hydrogel interface in hydrogel-based artificial skins. To demonstrate the excellent adhesion between the dielectric elastomer and ICE, we make a polymer string—which consists of two ICEs connected by a dielectric elastomer via junctions—by simply attaching the dielectric elastomer to the surface of the ICEs (Figure 4b–I). The elastomer-ICE interfaces are stable and sufficiently strong to sustain a weight of 200 g (Figure 4b-II). Besides the leakage-free nature and strong interfaces, both the conductive and dielectric layers of the novel ionic skin are of similar mechanical properties, largely reducing the mechanical mismatch common to capacitive sensors made of elastomers and conductive gels. Unlike many previous artificial skins that can only sense deformation,[11,12,49] the ionic skin in this work can achieve a variety of sensory capabilities toward multiple stimuli such as strain, force, and temperature (Figure 4c–e), mimicking the function of human skins. When the ionic skin is stretched or pressed, the effective area of the capacitor increases, inducing the increase in capacitance. Notably, taking advantage of the high modulus of the ICE, the novel ionic skin can sense a wide range of pressure up to several MPa (Figure 4d), whereas most gel-based ionic skins can only detect pressure in the range of 1 to 100 kPa.[11] We further apply the ionic skin to monitor a series of intermittent stimuli, including stretching (Figure 4f and Video S4, Supporting Information) and pressing (Figure 4g and Video S5, Supporting Information). The capacitive sensor shows fast response upon deformation and quick recovery when the force is released, with short response and recovery time. For example, the ionic skin can sense three consecutive gentle touches in ≈1 s (Inset, Figure 4g). The capacitive sensor system also demonstrates capability of temperature sensing (Figure S14, Supporting Information), since temperature change may affect the conductivity of the ICE as well as the dielectric constant of the dielectric layer, synergistically leading to the capacitance change of the ionic skin. We also report an ICE-based TENG, an energy harvester that is enabled by the coupling of contact electrification and electrostatic induction (Figure S15, Supporting Information). When touched by fingers, the TENG generates a peak current value of ≈0.4 μA and a peak voltage value of ≈4 V (Figure S16 and Video S6, Supporting Information).

Another advantage of our material is the 3D printability. 3D printing of gel-based ionic conductors have been extensively studied,[20,50] whereas liquid-free ICEs have not been printed yet. Herein, we develop a bottom-up digital light processing (DLP) 3D printing system (**Figure 5**a). The material used for printing is the precursor solution of the ICE added with 1% (v/v) poly(ethylene glycol) diacrylate (MW ≈700) as the crosslinker and 1% (v/v) ethyl (2,4,6-trimethylbenzoyl) phenylphosphinate (TPO-L) as the photoinitiator. The ICE can be printed to form various 2D and 3D shapes. For example, we print a 2D owl pattern with fine features (Figure 5b). The zoomed-in view of the owl's wing shows that the average width of the printed stripes is ≈160 μm (Figure 5c), demonstrating high printing resolution. Other 2D shapes such as a snowflake and an ICE circuit are also fabricated via printing (Figure 5d,e). Moreover, we print a complex 3D structure, a chess piece (Figure 5f), to demonstrate the good 3D printability of the liquid-free ICE. The printed structures are conductive (Table S6, Supporting Information).

In this study, we have demonstrated a liquid-free ICE that consists entirely of crosslinked long-chain copolymer networks and lithium salts. The material shows extraordinary mechanical versatility in terms of exceptional stretchability, high modulus/strength/toughness, unprecedented work of fracture, self-healing, quick self-recovery, and 3D-printability. Surprisingly, we find both strength and toughness of the ICE increase as the concentration of lithium salt increases, overcoming the well-recognized conflict between strength and

© 2021 Wiley-VCH GmbH

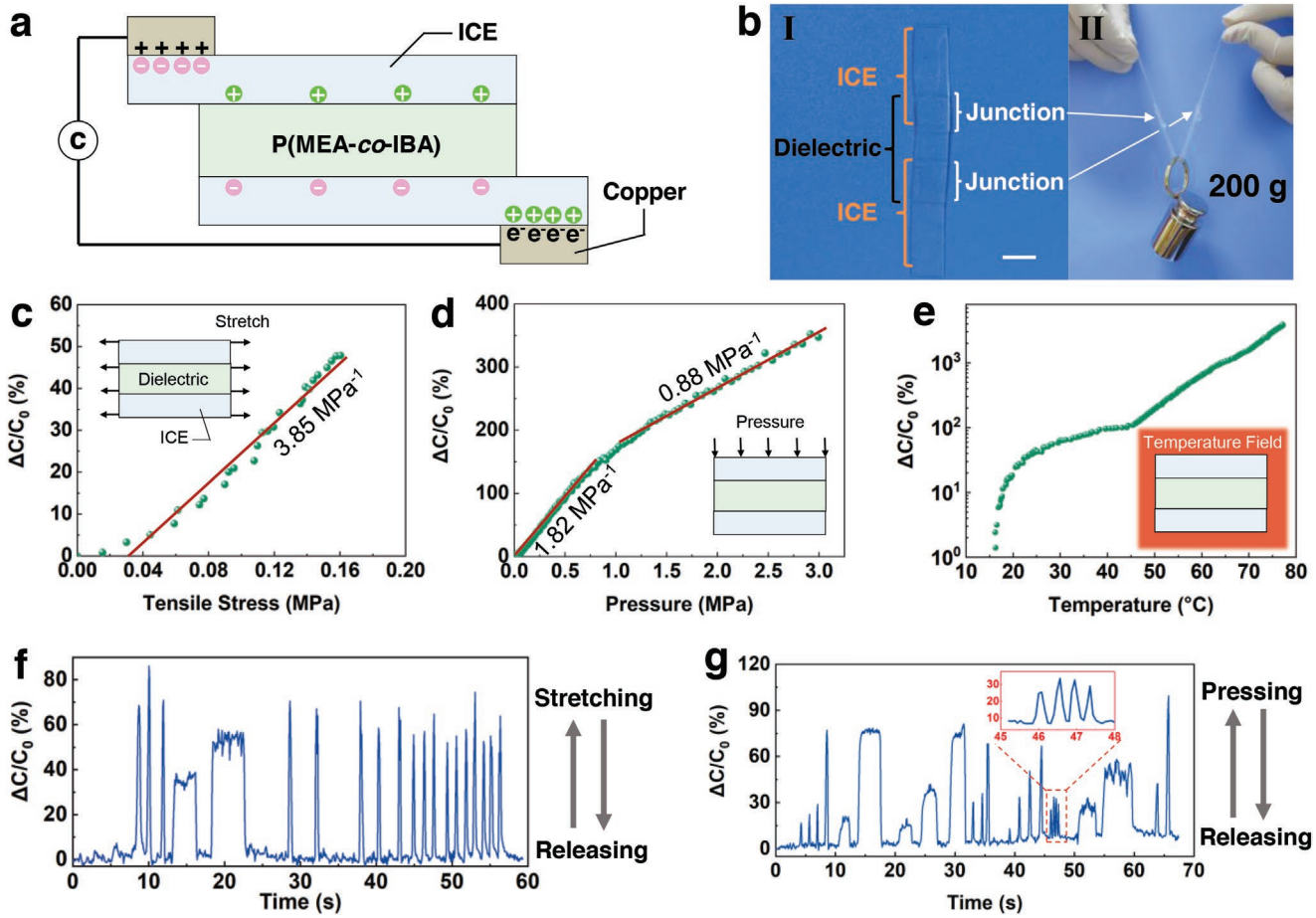

Figure 4. ICE-based liquid-free ionic skin that can sense strain, force, and temperature. a) Basic design of the ionic skin. Note that P(MEA-*co*-IBA) copolymer is utilized as the dielectric layer; The ICE, P(MEA-*co*-IBA) copolymer containing 1.5 M LiTFSI, is employed as the electrode. b) Photographs demonstrating the strong adhesion between the dielectric and conductive layers. (Scale bar: 1 cm) c) The measured capacitance–stretch curve. The sensitivity of the ionic skin in response to stretch is ≈3.85 MPa^{-1}. d) The measured capacitance–pressure curve. The ionic skin can sense a wide range of pressure up to several MPa. The sensitivity is ≈1.82 MPa^{-1} at low pressure while ≈0.88 MPa^{-1} when the pressure is high. e) The measured capacitance–temperature curve. f,g) The capacitance–time plot of an ionic skin subject to intermittent stretches (f) and touch motions (g). Inset: the ionic skin can recognize three consecutive touches in ≈1 s.

toughness—they are generally mutually exclusive. Moreover, mechanical properties and ionic conductivity can be simultaneously enhanced by increasing the concentration of lithium salts, successfully addressing the trade-off between the two properties for ionogels. The facile (re)formation of hydrogen bonds and lithium bonds between copolymer chains and lithium salts dispersed throughout the copolymer matrix is the underlying key to defeat the conflict of strength versus toughness and that between mechanical properties and ionic conductivity. We have demonstrated several ICE-based liquid-free ionotronic devices, including a resistive sensor, an ionic skin, and a triboelectric nanogenerator, which intrinsically do not suffer from leakage, evaporation, and weak hydrogel–elastomer interfaces—key impediments to stable operations of gel-based ionotronics. Processability of the ICE is further demonstrated via several 3D-printed objects such as a 2D owl pattern with fine features, and a 3D chess piece. This is, to our knowledge, the first investigation of the 3D printability of liquid-free ICEs. Taking advantage of its mechanical versatility, 3D printability, thermal stability, and optical transparency, the liquid-free ICE in this work offers promise for a variety of ionotronic devices that requires high environmental stability and durability.

Supporting Information

Supporting Information is available from the Wiley Online Library or from the author.

Acknowledgements

This research is supported by National Natural Science Foundation of China (Grant No. 11802269 and 12072314) and the One-Hundred Talents Program of Zhejiang University.

Conflict of Interest

The authors declare no conflict of interest.

© 2021 Wiley-VCH GmbH

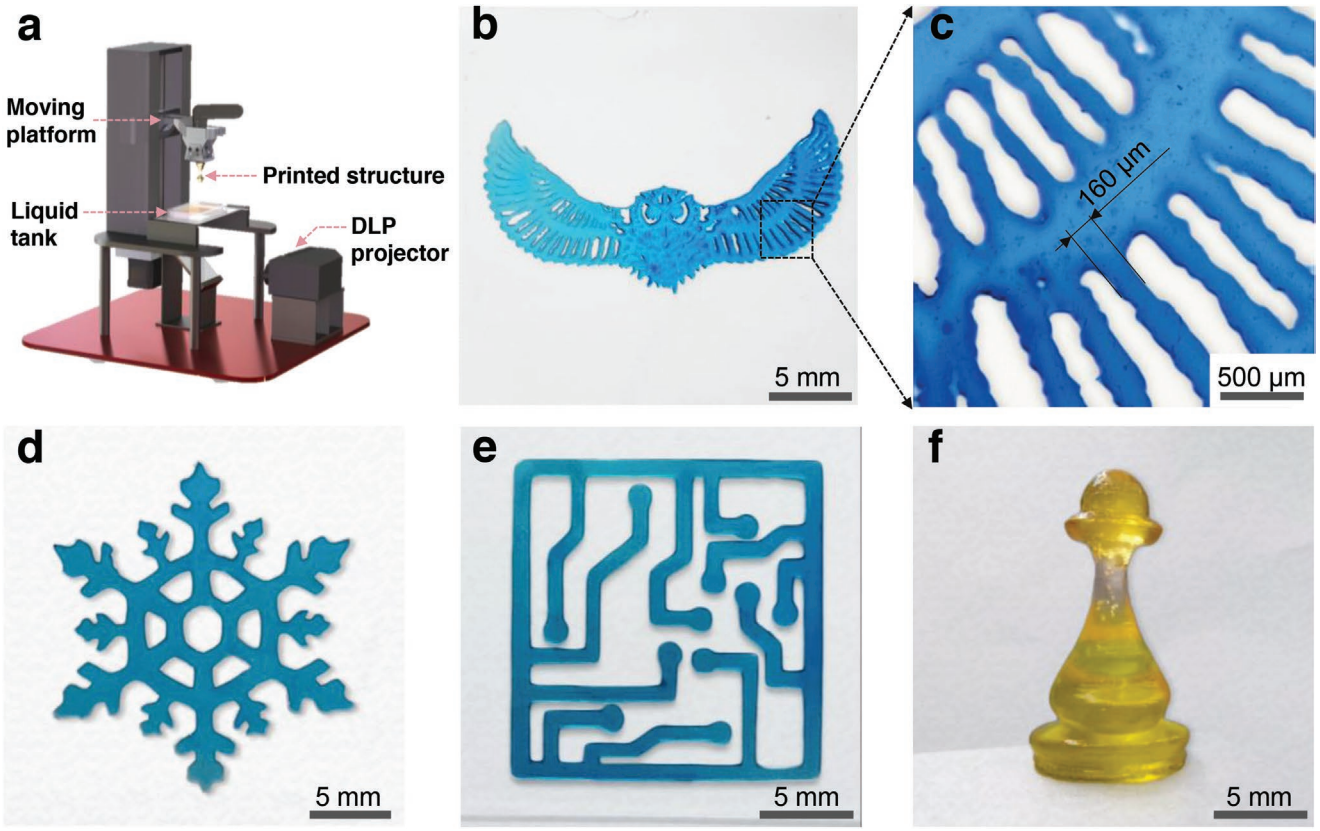

Figure 5. Demonstration of the printability of the liquid-free ICE. a) A DLP-based 3D printing system. The system is used to fabricate various 2D and 3D structures. b) A printed owl pattern. c) The zoomed-in view of the owl's wing, demonstrating high printing resolution of ≈160 µm. d) A printed snowflake. e) An ICE circuit. f) A 3D chess piece. The molar concentration of LiTFSI in all printed samples is $C = 0.5$ M.

Data Availability Statement

Research data are not shared.

Keywords

3D-printability, conductivity, ionic conductive elastomers, ionotronics, mechanical properties

Received: September 7, 2020
Revised: December 29, 2020
Published online:

[1] C. C. Kim, H. H. Lee, K. H. Oh, J. Y. Sun, *Science* **2016**, *353*, 682.
[2] Y. Xie, R. Xie, H. C. Yang, Z. Chen, J. Hou, C. R. Lopez-Barron, N. J. Wagner, K. Z. Gao, *ACS Appl. Mater. Interfaces* **2018**, *10*, 32435.
[3] L. Shi, K. Jia, Y. Gao, H. Yang, Y. Ma, S. Lu, G. Gao, H. Bu, T. Lu, S. Ding, *Research* **2020**, *2020*, 1.
[4] N. Bai, L. Wang, Q. Wang, J. Deng, Y. Wang, P. Lu, J. Huang, G. Li, Y. Zhang, J. Yang, K. Xie, X. Zhao, C. F. Guo, *Nat. Commun.* **2020**, *1*, 209.
[5] C. H. Yang, B. Chen, J. J. Lu, J. H. Yang, J. Zhou, Y. M. Chen, Z. Suo, *Extreme Mech. Lett.* **2015**, *3*, 59.
[6] T. Yin, L. Wu, T. Wu, G. Mao, G. Nian, Z. Chen, X. Hu, P. Wang, Y. Xiang, H. Yu, S. Qu, W. Yang, *J. Polym. Sci., Part B: Polym. Phys.* **2019**, *57*, 272.
[7] Y. Lee, S. H. Cha, Y. W. Kim, D. Choi, J. Y. Sun, *Nat. Commun.* **2018**, *9*, 1804.
[8] Y. Wang, Z. Wang, Z. Su, S. Cai, *Extreme Mech. Lett.* **2019**, *28*, 81.
[9] C. H. Yang, B. Chen, J. Zhou, Y. M. Chen, Z. Suo, *Adv. Mater.* **2016**, *28*, 4480.
[10] C. Yang, Z. Suo, *Nat. Rev. Mater.* **2018**, *6*, 125.
[11] J. Y. Sun, C. Keplinger, G. M. Whitesides, Z. Suo, *Adv. Mater.* **2014**, *26*, 7608.
[12] Z. Lei, Q. Wang, S. Sun, W. Zhu, P. Wu, *Adv. Mater.* **2017**, *29*, 1700321.
[13] B. Ying, Q. Wu, J. Li, X. Liu, *Mater. Horiz.* **2020**, *7*, 477.
[14] C. Keplinger, J. Y. Sun, C. C. Foo, P. Rothemund, G. M. Whitesides, Z. Suo, *Science* **2013**, *341*, 984.
[15] X. Pu, M. Liu, X. Chen, J. Sun, C. Du, Y. Zhang, J. Zhai, W. Hu, Z. L. Wang, *Sci. Adv.* **2017**, *3*, e1700015.
[16] K. Parida, V. Kumar, W. Jiangxin, V. Bhavanasi, R. Bendi, P. S. Lee, *Adv. Mater.* **2017**, *29*, 1702181.
[17] R. H. Stokes, R. A. Robinson, *J. Am. Chem. Soc.* **1947**, *70*, 1870.
[18] B. Chen, J. J. Lu, C. H. Yang, J. H. Yang, J. Zhou, Y. M. Chen, Z. Suo, *ACS Appl. Mater. Interfaces* **2014**, *10*, 7840.
[19] Q. Liu, G. Nian, C. Yang, S. Qu, Z. Suo, *Nat. Commun.* **2018**, *9*, 846.
[20] H. Yang, C. Li, M. Yang, Y. Pan, Q. Yin, J. Tang, H. J. Qi, Z. Suo, *Adv. Funct. Mater.* **2019**, *29*, 1901721.
[21] Y. Ren, J. Guo, Z. Liu, Z. Sun, Y. Wu, L. Liu, F. Yan, *Sci. Adv.* **2019**, *5*, eaax0648.
[22] Y. M. Kim, H. C. Moon, *Adv. Funct. Mater.* **2019**, *30*, 1907290.
[23] D. M. Correia, L. C. Fernandes, P. M. Martins, C. García-Astrain, C. M. Costa, J. Reguera, S. Lanceros-Méndez, *Adv. Funct. Mater.* **2020**, *30*, 1909736.

© 2021 Wiley-VCH GmbH

[24] Y. Cao, T. G. Morrissey, E. Acome, S. I. Allec, B. M. Wong, C. Keplinger, C. Wang, *Adv. Mater.* **2017**, *29*, 1605099.
[25] Z. Lei, P. Wu, *Nat. Commun.* **2019**, *10*, 3429.
[26] Z. Cao, H. Liu, L. Jiang, *Mater. Horiz.* **2020**, *7*, 912.
[27] B. C. Hyeong Jun Kim, Z. Suo, R. C. Hayward, *Science* **2020**, *367*, 773.
[28] P. Zhang, Y. Chen, Z. H. Guo, W. Guo, X. Pu, Z. L. Wang, *Adv. Funct. Mater.* **2020**, *30*, 1909252.
[29] L. Shi, T. Zhu, G. Gao, X. Zhang, W. Wei, W. Liu, S. Ding, *Nat. Commun.* **2018**, *9*, 2630.
[30] L. Long, S. Wang, M. Xiao, Y. Meng, *J. Mater. Chem. A* **2016**, *4*, 10038.
[31] H. Zhu, S. Zhu, Z. Jia, S. Parvinian, Y. Li, O. Vaaland, L. Hu, T. Li, *Proc. Natl. Acad. Sci., USA* **2015**, *112*, 8971.
[32] R. O. Ritchie, *Nat. Mater.* **2011**, *10*, 817.
[33] L. Chen, T. L. Sun, K. Cui, D. R. King, T. Kurokawa, Y. Saruwatari, J. P. Gong, *J. Mater. Chem. A* **2019**, *7*, 17334.
[34] Y. Ding, J. Zhang, L. Chang, X. Zhang, H. Liu, L. Jiang, *Adv. Mater.* **2017**, *29*, 1704253.
[35] J. Li, W. R. K. Illeperuma, Z. Suo, J. J. Vlassak, *ACS Macro Lett.* **2014**, *3*, 520.
[36] D. G. Mackanic, X. Yan, Q. Zhang, N. Matsuhisa, Z. Yu, Y. Jiang, T. Manika, J. Lopez, H. Yan, K. Liu, X. Chen, Y. Cui, Z. Bao, *Nat. Commun.* **2019**, *10*, 5384.
[37] J. Lee, M. W. M. Tan, K. Parida, G. Thangavel, S. A. Park, T. Park, P. S. Lee, *Adv. Mater.* **2020**, *32*, 2070048.
[38] C. Yang, T. Yin, Z. Suo, *J. Mech. Phys. Solids* **2019**, *131*, 43.
[39] C. Chen, Z. Wang, Z. Suo, *Extreme Mech. Lett.* **2017**, *10*, 50.
[40] X. Chen, Y. K. Bai, C. Z. Zhao, X. Shen, Q. Zhang, *Angew. Chem., Int. Ed.* **2020**, *59*, 11192.
[41] Y. Shi, M. Wang, C. Ma, Y. Wang, X. Li, G. Yu, *Nano Lett.* **2015**, *15*, 6276.
[42] M. A. Darabi, A. Khosrozadeh, R. Mbeleck, Y. Liu, Q. Chang, J. Jiang, J. Cai, Q. Wang, G. Luo, M. Xing, *Adv. Mater.* **2017**, *29*, 1700533.
[43] S. Liu, L. Li, *ACS Appl. Mater. Interfaces* **2017**, *9*, 26429.
[44] S. H. Zhang, F. X. Wang, J. J. Li, H. D. Peng, J. H. Yan, G. B. Pan, *Sensors* **2017**, *17*, 2621.
[45] C. Shao, M. Wang, L. Meng, H. Chang, B. Wang, F. Xu, J. Yang, P. Wan, *Chem. Mater.* **2018**, *30*, 3110.
[46] J. Lai, H. Zhou, Z. Jin, S. Li, H. Liu, X. Jin, C. Luo, A. Ma, W. Chen, *ACS Appl. Mater. Interfaces* **2019**, *11*, 26412.
[47] Q. Zhang, X. Liu, X. Ren, F. Jia, L. Duan, G. Gao, *Chem. Mater.* **2019**, *31*, 5881.
[48] X. Zhang, N. Sheng, L. Wang, Y. Tan, C. Liu, Y. Xia, Z. Nie, K. Sui, *Mater. Horiz.* **2019**, *6*, 326.
[49] Z. Qiu, Y. Wan, W. Zhou, J. Yang, J. Yang, J. Huang, J. Zhang, Q. Liu, S. Huang, N. Bai, Z. Wu, W. Hong, H. Wang, C. F Guo, *Adv. Funct. Mater.* **2018**, *28*, 1802343.
[50] Z. Chen, D. Zhao, B. Liu, G. Nian, X. Li, J. Yin, S. Qu, W. Yang, *Adv. Funct. Mater.* **2019**, *29*, 1900971.

© 2021 Wiley-VCH GmbH